HAPTIC INTERFACE OPTIMIZATION FOR VIRTUAL ANASTOMOSIS SURGERY TRAINING

by

KANGJI HUANG

Presented to the Faculty of the Graduate School of
The University of Texas at Arlington in Partial Fulfillment
of the Requirements for the Degree of

MASTER OF SCIENCE

in

MECHANICAL ENGINEERING

THE UNIVERSITY OF TEXAS AT ARLINGTON

August 2021

ACKNOWLEDGEMENTS

First of all, I would like to thank my supervising professor Dr. Alan Bowling and Dr. Ganesh Sankaranarayanan for providing me a chance to perform this research and constantly motivating and encouraging me. Especially thank Dr. Bowling for igniting my interest in dynamics and robotics. I would like to thank Dr. Robert Taylor and Dr. Shou Wang for being on my defense committee members and providing their time and expertise in reviewing my work.

I would also like to thank my mentors, Vatsal Joshi and Manoochehr Rabiei for keeping inspiring me during the time of my research and providing me numerous advice for my master's study.

Finally, I am very grateful to my parents who have always encouraged and supported me throughout my college life. I couldn't get this far without their help.

Aug 11, 2021

ABSTRACT

HAPTIC INTERFACE OPTIMIZATION FOR VIRTUAL ANASTOMOSIS SURGERY TRAINING

KANGJI HUANG, M.S.

The University of Texas at Arlington, 2021

Supervising Professor: Alan P. Bowling

Virtual anastomosis surgery study allows surgeons to perform or practice suturing in virtual reality using a commercial haptic device. The haptic device can generate force feedback so that the user can feel the real touch sensation of the object in virtual reality. The virtual anastomosis surgery study has two requirements which are that the haptic device must be fixed on the operating table and haptic device location must be suitable for different surgeons. The goal is to use a commercially available haptic device for this purpose, rather than design a new device for each possible surgery that must be performed. Therefore, it is necessary to do placement optimization to find the best position and orientation that would allow several surgeons to train using those devices.

There are 16 different surgeons who participated and provided their surgery data for the optimization. The first step in this work involved measuring the workspace required for surgery. An electromagnetic tracking system was used to track the position of surgeons' hands when they were performing the suturing. The second step was to model the haptic device to determine its workspace and possible motions. The third

was to use optimization to find the position and orientation of the haptic device that would allow the greatest coverage of workspace measured from the surgeons. The fourth step involved performing a dynamic simulation of the haptic device to check for collisions between the haptic device as the surgeons move through the trajectories used to determine the measured workspace. Finally, some preliminary testing was done with actual surgeons to validate whether this process is useful for the haptic interface design.

TABLE OF CONTENTS

LIST OF ILLUSTRATIONS

LIST OF TABLES

CHAPTER 1

INTRODUCTION

Virtual reality (VR) is becoming a popular new tool for medical applications, and it has been rapidly developed in this decade [9]. The application field is divided into two main parts: telesurgery [18] and medical training [5]. For example, in the area of medical education, simulation using VR technology can be used to palpate the patient's virtual liver to search for hard regions beneath the surface [4]. In addition, the real-time suturing simulation for medical training allows surgeons to practice suturing on a virtual operation table [22].

In reality, surgery or patient examination requires doctors or surgeons use force feedback to determine patients' condition or perform an operation. In virtual reality, the haptic interaction can help to improve the immersion of the operator [11]. Therefore, the simulator should be able to provide haptic force feedback according to different surgery and interaction with the patients. The medical simulator designed for suturing operation can produce force feedback for some fundamental skills, such as suturing and cutting [22].

The haptic device iFeel3 was developed by a research team at Beihang University in China. It allows dentists to feel forces while performing dental surgery [11]. There are some commercial haptic devices that are also used for surgery simulation. The research team at Thammasat University in Thailand used the PHANTOM Omni for telesurgery [17] and another research group in Germany used the KUKA LBR iiwa Robot as the haptic device to perform hip replacement surgery [15].

Custom designed haptic devices are particular to a specific surgery, and they guarantee that surgeons can access the surgery workspace without any restrictions. For example, the haptic device iFeel3 was prototyped for the simulation of dental surgery such that its workspace could cover the entire oral cavity [11]. Commercial haptic devices are more cost-effective and efficient compared with custom designed ones. However, the commercial haptic device may have limitations owing to insufficient workspace so that some critical regions for performing surgery are unreachable [10]. Therefore, it is necessary to optimize the placement of commercial devices to cover a sufficient amount of the surgery workspace.

1.1 Virtual Anastomosis Surgery Study

The goal of virtual anastomosis surgery study is to optimize the placement of two haptic devices for best use in performing suturing in a virtual reality simulation. The study is aimed at allowing users to practice suturing in virtual reality with a simple system setup. Users can visually detect and interact with the object by wearing a VR device and manipulating virtual objects with a haptic device. The VR device and the haptic device are commercial products which ensure quick installation and ease of use.

The Hand Sewn Anastomosis Study has two requirements of haptic device. The first requirement is the haptic device must be fixed on the operating table. Once the location of haptic device is fixed, the workspace of the haptic device is also fixed. The workspace of the commercial haptic device is not custom designed for this hand sewn anastomosis study, so some of the surgery workspace may not be covered by the haptic device. The second requirement is the location for placing the haptic device should be suitable for several different surgeons. Different surgeons may perform the same surgery differently, imposing more complex workspace requirements on the device.

Placement optimization for task execution is a very common study. A research group in Michigan provides a method for optimizing the base position of an industrial robot with the objective to reach all predefined task and minimize the cycle time [20]. The cost function they used is the number of tasks that can be executed by the robot. For this work, 16 different surgeons participated and provided their own surgery workspace. The workspace of two the commercially available haptic devices were modeled and used to maximize their coverage of the measured workspace. A simulation of the device was then used to move the haptic device through the surgery paths used to define the measured workspace to determine whether the devices would collide with each other. Finally, some preliminary testing was done to determine whether actual surgeons could effectively utilize the optimal device placements to perform anastomosis surgery.

CHAPTER 2

Hardware

2.1 3D SYSTEM Touch Haptic Device

The Touch haptic device is the commercially available, produced by the company 3D SYSTEM. This haptic device has 6 degrees of freedom (DOFs) position sensing and 3 DOFs force feedback to allow the user to feel virtual objects. While the surgeon is manipulating the haptic device, the end-effector position can be determined using the forward kinematic equation and the current angle of each joint. The current position of the end-effector can be projected onto the virtual environment. Once the end-effector has interacted with the virtual object, the interaction forces can be detected and converted to joint torques applied on each joint to produce a force feedback to the surgeon. Figure 2.1 presents different components of the haptic device. Link A (Head), link B (Crank) and link C (Connecting Rod) include force feedback, and link D (Wrist), E (Fork), and F (Connector) do not participate the force transmission. Each joint angle is measured relative to the previous link, and they are designated as q_1, q_2, q_3, q_4, q_5, and q_6. The limits on each joint angle are given in Table 2.1. Notice that the joint limit on q_3 is dependent on the current position of joint 2, q_2 [12].

In Equation (2.3) below, as the value of q_2 (angle between link A and link B) ranges from 0° to 50°, q_3 remains constant which ranges from -20° to -145°. The

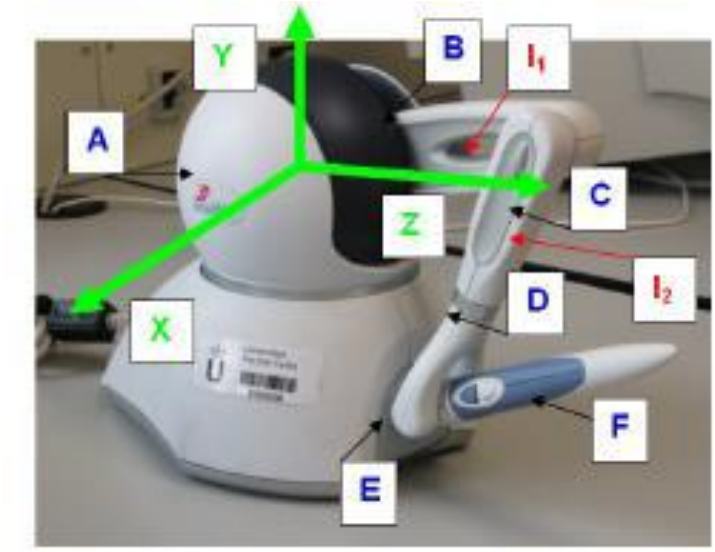

Figure 2.1: Different Components of the Haptic Device

Joint Angles	Upper Bound	Lower Bound
q_1	$-50°$	$55°$
q_2	$0°$	$105°$
q_3	$-20°$	$-145°$
q_4	$-170°$	$170°$
q_5	$0°$	$160°$
q_6	$-170°$	$170°$

Table 2.1: Joint Limits

angles $q_{2,1}$ and $q_{2,2}$ determine the region of q_2. As q_2 goes from $q_{2,1}$ to $q_{2,2}$, the upper bound of q_3 will change based on the current angle of q_2:

$$Ratio = \frac{q_{3,ub}|_{q_2=50} - q_{3,ub}|_{q_2=105}}{q_{2,1} - q_{2,2}}, \tag{2.1}$$

$$Ratio = \frac{-20 - (-80)}{50 - 105} = -1.09, \tag{2.2}$$

$$q_{3,ub}|_{new} = -20 + Ratio \times (q_2 - 50)\,. \tag{2.3}$$

2.2 Electromagnetic Tracking System

The Electromagnetic Tracking System was used to measure the actual workspace necessary for surgery [21]. It has three main components: the electronics unit, sensors, and transmitter. The transmitter creates electromagnetic field (EMF) in a rectangular region with dimensions 600 H $\times$ 560 W $\times$ 460 D mm as shown in Figure 2.2 [6]. The rectangular region is 200 mm in front of the transmitter. The transmitter can track their current position and orientation of its sensors with respect to its own location and orientation. Figure 2.3 shows the body attached frame for the transmitter and the sensors [6].

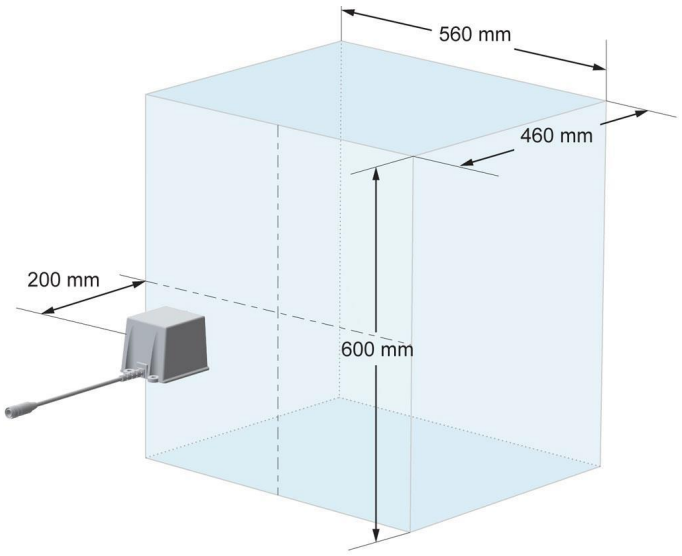

Figure 2.2: Measurement Volume of Transmitter [6]

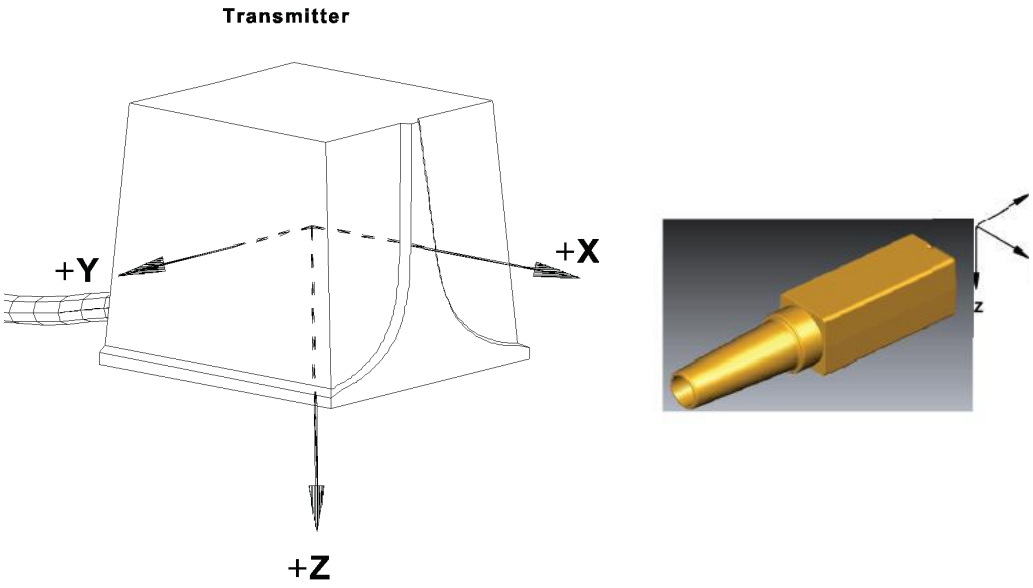

Figure 2.3: The Body Attached Frame of Transmitter and Sensor [6]

CHAPTER 3

Optimal Haptic Device Location

3.1 Measuring the workspace for the surgery

The first step in this work is to measure the actual workspace necessary for the surgery. Figure 3.1 shows the arrangement on the operating table. The transmitter is placed in front of the surgeon and its measurement volume could cover the surgery workspace on the operating table. The holder is fixed on the operating table and silicon tubes are mounted on the holder. Sensors are mounted on the back of hands.

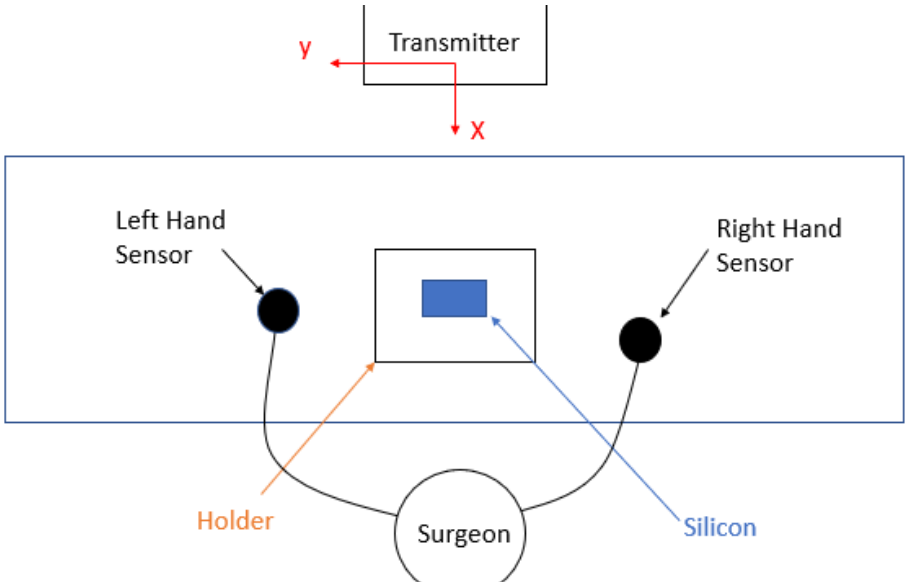

Figure 3.1: The Arrangement of Operating Table

Once the sensors move inside the measurement volume, the position and orientation of the sensor are recorded. To visualize the surgery workspace, we plotted

position records of both hands in MATLAB. Figure 3.2 shows the positions recorded combining 16 surgery workspace performed by 16 different surgeons. The surgery workspace of both hands are separated, as indicated by different colors. The green volume and blue volume show the workspace of the left hand and the right hand.

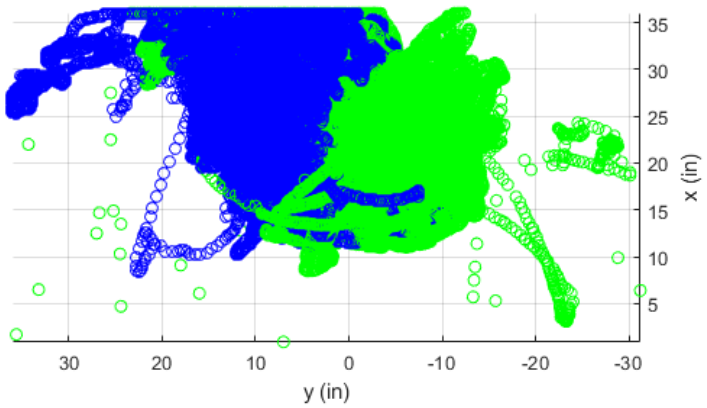

Figure 3.2: The Surgery Workspace

3.2 Theoretical Workspace of The Commercial Haptic Device

The second step is to model the haptic device to determine its workspace and possible motions. The dynamic model and motion simulation of the haptic device will be introduced in Chapter 4. In this section, the introduction will mainly focus on the process for defining the haptic device workspace.

The haptic device is composed of 6 rotational joints. Each rotational joint has its own range. The range of the third joint is dependent on the current position of the second joint. Table 2.1 and Equation (2.3) present the range of each joint and the joint constraint equation between the second and the third joints. The range of each joint can be equally divided into 6 angles. These 46656 combinations were substituted into

the forward kinematic equation to compute the position of the end-effector. These positions generate a representation of the haptic device workspace. Figure 3.3 shows the haptic device workspace after plotting all the end-effector positions.

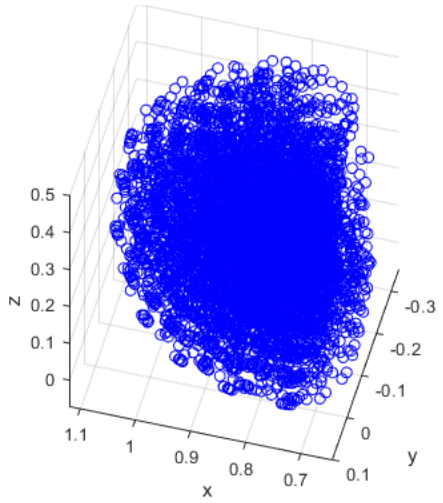

Figure 3.3: The End-Effector Point

In reality, there are some end-effector positions that are not reachable because the arm (Link C, D, E, and F) can collide with the base (Link A and B) before reaching these positions. Therefore, the physical volume of the base should be considered to define the correct haptic device workspace. In Figure 3.4, the base was represented by a rectangular box of dimension 0.25 W×0.35 H×0.21 D m. The position points inside the box may cause the self collision, and thus are removed before visualizing the workspace.

Once those position points are removed, the triangular mesh can be created by computing a Delaunay triangulation connectivity for the left position points using the delaunay function in MATLAB. The triangular mesh generates a closed volume which indicates the workspace of the haptic device. Figure 3.5 shows the theoretical workspace of the haptic device.

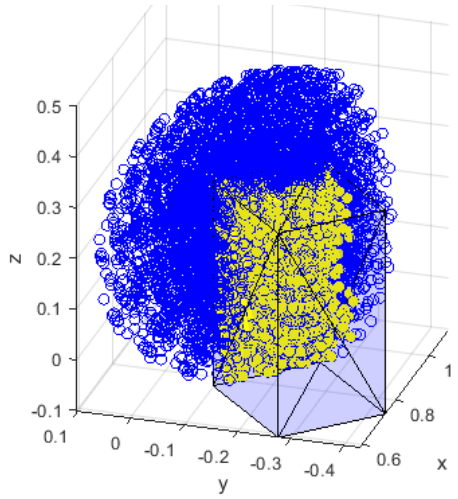

Figure 3.4: The End-Effector Points Overlapped by The Haptic Device

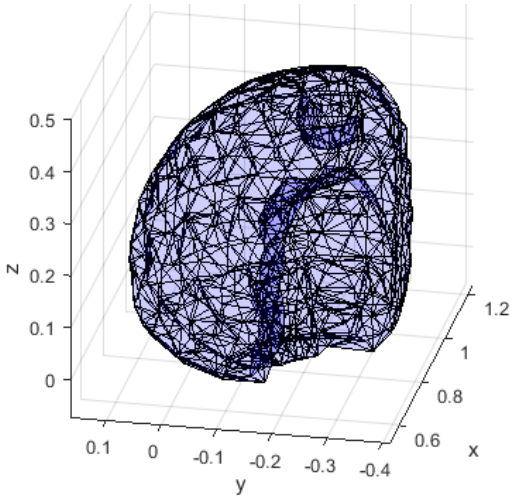

Figure 3.5: The Theoretical Workspace of the Haptic Device

3.3 The Placement Optimization of Haptic Device

The third step is to use optimization to find the position and orientation of the haptic device that allow the greatest coverage of workspace measured from the surgeons. There are four variables for optimization, which are X, Y, Z, and θ. The X, Y, Z are the coordinates which indicates the location of device, and θ is the base angle which indicates its orientation. It is important to know the initial guess,

variable bounds, and cost function before starting optimization. Figure 3.6 shows the top view of the surgery workspace with the haptic devices that are placed to their initial positions and orientations. Table 3.1 shows the specific initial location and base angle for each device.

Variables	Left-Hand Device	Right-Hand Device
X	$0.508m$	$0.762m$
Y	$0.254m$	$-0.254m$
Z	$0m$	$0m$
θ	$135°$	$-45°$

Table 3.1: Initial Guess

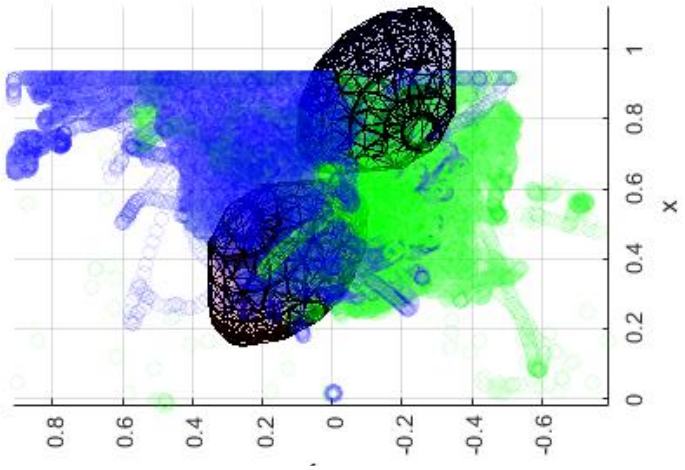

Figure 3.6: Initial Guess for Optimization

It is also important to define the upper and lower bounds for each variable. Figure 3.7 shows the top view of the operating table with the boundary of the left-

hand and the right-hand device on x-y plane. The specific boundary values are given in Table 3.2

Variables	LowerBound	UpperBound
$X\,(Left)$	$0.254m$	$0.762m$
$Y\,(Left)$	$0.127m$	$0.381m$
$Z\,(Left)$	$0m$	$0.127m$
$\theta\,(Left)$	$0°$	$360°$
$X\,(Right)$	$0.381m$	$0.762m$
$Y\,(Right)$	$-0.508m$	$0m$
$Z\,(Right)$	$0m$	$0.127m$
$\theta\,(Right)$	$0°$	$360°$

Table 3.2: Boundary Values

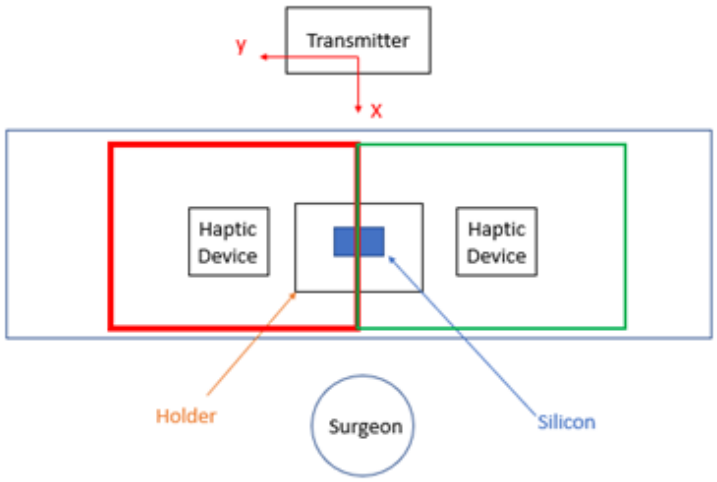

Figure 3.7: The Location of The Haptic Device

The final step is to define a cost function for the optimization. To maximize the coverage of surgery workspace, a sufficient amount of the position data recorded form the surgeons should be covered by the haptic device workspace. Figure 3.8 shows an example of the coverage of the surgery workspace. Equation (3.1) shows the cost function for the optimization is

$$Cost = \sum_{i=1}^{n} d_i^2 = d_1^2 + d_2^2 + d_3^2 + \cdots + d_n^2, \tag{3.1}$$

where d_i is the shortest distance from the position points outside the workspace to the surface of the workspace, and n is the total number of the position points outside the workspace. By minimizing this sum of distances, the workspace will cover more position points measure from the surgeons, which results in the increasing of the coverage of the surgery workspace.

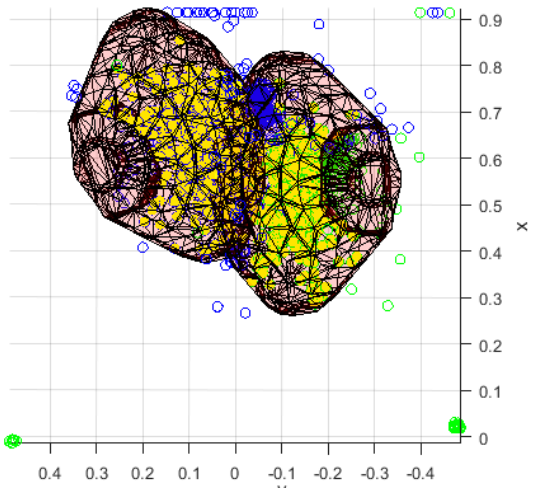

Figure 3.8: The Coverage of The Surgery Workspace

CHAPTER 4

Dynamic Model

The workspace of the haptic device was defined in Chapter 3. In this chapter, The dynamic model is created to determine the possible motions of the haptic device. The motions of the haptic device follow the trajectories provided by the position records measured from the surgeons.

According to the position records, the inverse kinematics can calculate the angles of each joint to determine the configuration for reaching these position records [19], [7]. However, the inverse kinematics cannot guarantee that these configurations can generate a continuous motion representing execution of the surgical task.

The operational space control is able to plan a trajectory that can directly move the end-effector between two positions [8]. The joint limits were applied to the operational space control to push the link backward as it hits the joint limit.

4.1 Equation of Motion and Operational Space Control

The general form of equation of motion is [1]

$$A(\mathbf{q})\ddot{\mathbf{q}} + \mathbf{b}(\mathbf{q}, \dot{\mathbf{q}}) = \mathbf{g}(\mathbf{q}) + \boldsymbol{\gamma}, \tag{4.1}$$

where A is the mass matrix, $\mathbf{b}$ is a vector containing velocity dependent terms, $\mathbf{g}$ is a vector containing gravitational forces, $\boldsymbol{\gamma}$ is the vector of generalized active forces which are the joint torques, and $\mathbf{q}$ is the vector of generalized coordinates which refer to characterizations of the system that uniquely defines its configuration. The haptic

device has 6 DOFs which means that there are 6 independent generalized coordinates in

$$\mathbf{q} = [q_1 \; q_2 \; q_3 \; q_4 \; q_5 \; q_6]^T . \tag{4.2}$$

Accordingly, $\dot{\mathbf{q}}$ and $\ddot{\mathbf{q}}$ are vectors of the first and second order derivatives of the generalized coordinates, respectively, as in Equations (4.3) and (4.4):

$$\dot{\mathbf{q}} = [\dot{q}_1 \; \dot{q}_2 \; \dot{q}_3 \; \dot{q}_4 \; \dot{q}_5 \; \dot{q}_6]^T , \tag{4.3}$$

$$\ddot{\mathbf{q}} = [\ddot{q}_1 \; \ddot{q}_2 \; \ddot{q}_3 \; \ddot{q}_4 \; \ddot{q}_5 \; \ddot{q}_6]^T . \tag{4.4}$$

Equation (4.5) below reveals a property of the Jacobian J: J^T transforms end-effector forces and moments, $\mathbf{F}$, to generalized active forces, $\boldsymbol{\gamma}$,as

$$\boldsymbol{\gamma} = J^T(\mathbf{q})\mathbf{F}. \tag{4.5}$$

Due to the duality of the Jacobian matrix, the Jacobian also transforms the generalized velocity vector, $\dot{\mathbf{q}}$, to end-effector velocities, $\dot{\mathbf{x}}$,as

$$\dot{\mathbf{x}} = J(\mathbf{q})\dot{\mathbf{q}}. \tag{4.6}$$

The second order derivative of the end-effector velocities, $\ddot{\mathbf{x}}$, can be computed by differentiating Equation (4.6) to get

$$\ddot{\mathbf{x}} = \dot{J}\dot{\mathbf{q}} + J\ddot{\mathbf{q}}. \tag{4.7}$$

By isolating $\ddot{\mathbf{q}}$, we have

$$J\ddot{\mathbf{q}} = \ddot{\mathbf{x}} - \dot{J}\dot{\mathbf{q}}, \tag{4.8}$$

$$\ddot{\mathbf{q}} = J^{-1}\left(\ddot{\mathbf{x}} - \dot{J}\dot{\mathbf{q}}\right). \tag{4.9}$$

By substituting Equation (4.9) into Equation (4.1), the generalized active force, $\boldsymbol{\gamma}$, can be related to the end-effector acceleration, $\ddot{\mathbf{x}}$,as

$$\gamma = A(\mathbf{q})J^{-1}\left(\ddot{\mathbf{x}} - \dot{J}\dot{\mathbf{q}}\right) + \mathbf{b}(\mathbf{q}, \dot{\mathbf{q}}) - \mathbf{g}(\mathbf{q}).$$

The generalized active forces are the joint torques applied to each joint of the haptic device, and $\ddot{\mathbf{x}}$ can be defined using a basic proportional and derivative (PD) controller [14]. Equation (4.1) shows the mathematic equation of a PD controller [16],

$$\ddot{\mathbf{x}} = k_p \left(\mathbf{x}_{des} - \mathbf{x} \right) + k_v \left(\dot{\mathbf{x}}_{des} - \dot{\mathbf{x}} \right), \tag{4.10}$$

where k_p and k_v are the proportional and derivative gains. The desire position and orientation of the end-effector are characterized by $\mathbf{x}_{des}$ and $\dot{\mathbf{x}}_{des}$. The operational space control allows the dynamic system to plan a trajectory that is directly relevant to the desire position. To make the end-effector be settled as it approaches to the desire position, the desired velocity of the translation and rotation, $\dot{\mathbf{x}}_{des}$, should be equal to zero. The desire acceleration, $\ddot{\mathbf{x}}$, of the end-effector will be substituted into the general form of the equation of motion to calculate the joint torques such that the haptic device can maintain a certain configuration to reach the desire position.

The sensors' data contain the desired translation and rotation of the end-effector. However, including rotation control will increase the complexity and difficulty of the simulation. Therefore, this dynamic model will focus on the end-effector position control. In Equation (4.11), the desired positions are X_{des}, Y_{des}, and Z_{des} determine and the orientation error is set equal to zero:

$$\mathbf{x}_{des} = \left[X_{des} \; Y_{des} \; Z_{des} \; 0 \; 0 \; 0 \right]^T. \tag{4.11}$$

4.2 Operational Space Formulation to Enforce Joint Limit

Most of the time, the trajectory planed by the operational space control is just a straight line in each dimension. However, it is not possible to always have a straight line between two positions due to the joint limits of the haptic device. The joint limits should be applied to the operational space control in order to simulate the correct motion of the haptic device.

As the joint hits its boundary, the joint limit is activated and generate a repulsive force to push the joint away from the limit. The joint torques $\boldsymbol{\gamma}$ calculated by Equation (4.1) needs to be projected onto a null space matrix. Null space matrix N_{lim} will remove the torque from the joint which hits its joint limit [13],[3]. In Equation (4.12)

$$\boldsymbol{\gamma}_c = \boldsymbol{\gamma}_{lim} + N_{lim}\boldsymbol{\gamma}, \tag{4.12}$$

where $\boldsymbol{\gamma}_{lim}$ is the vector of repulsive forces converted into joint torques and $\boldsymbol{\gamma}_c$ is the vector of the joint torques which is applied to each joint while the joint limits are activated. In Equation (4.13) and (4.14) $\mathbf{q}$ is the joint coordinate with its upper bound $\overline{\mathbf{q}}$, and lower bound $\underline{\mathbf{q}}$. $\overline{\boldsymbol{\rho}}$ and $\underline{\boldsymbol{\rho}}$ are differences between the current joint angle and its two boundary values:

$$\underline{\boldsymbol{\rho}} = \mathbf{q} - \underline{\mathbf{q}}, \tag{4.13}$$

$$\overline{\boldsymbol{\rho}} = \overline{\mathbf{q}} - \mathbf{q}, \tag{4.14}$$

where $\mathbf{q}$ is the joint coordinate with its upper bound $\overline{\mathbf{q}}$, and lower bound $\underline{\mathbf{q}}$, and $\overline{\boldsymbol{\rho}}$ and $\underline{\boldsymbol{\rho}}$ are differences between the current joint angle and its two boundary values.

In Equation (4.15) and (4.16)

$$f_{\underline{\rho}i} = \begin{cases} \eta\left(\frac{1}{\underline{\rho}_i} - \frac{1}{\underline{\rho}_0}\right)\frac{1}{\underline{\rho}_i^2}, & \text{if} \quad \underline{\rho}_i \leq \underline{\rho}_0, \\ 0, & \text{if} \quad \underline{\rho}_i \geq \underline{\rho}_0, \end{cases} \tag{4.15}$$

$$f_{\overline{\rho}i} = \begin{cases} \eta\left(\frac{1}{\overline{\rho}_i} - \frac{1}{\overline{\rho}_0}\right)\frac{1}{\overline{\rho}_i^2}, & \text{if} \quad \overline{\rho}_i \leq \overline{\rho}_0, \\ 0, & \text{if} \quad \overline{\rho}_i \geq \overline{\rho}_0, \end{cases} \tag{4.16}$$

the joint limit is designed to be activated when the joint reach a critical zone which is several degrees before the joint limit, where i is the index of the generalized coordinates, $\overline{\rho}_0$ and $\underline{\rho}_0$ determine the critical zone at the each of these joint limits, $f_{\overline{\rho}_i}$ and $f_{\underline{\rho}_i}$ are the corresponding repulsive forces that will be generated while the joint

is within the critical zone, and η is a constant gain such that higher value of η results in a faster increment of the repulsive force while the joint is coming to its joint limit. The term $\mathbf{f}$ is the general force vector that pushes the joint out of the critical zone, and it can be computed by summing the corresponding force vectors $\mathbf{f}_{\overline{\rho}}$ and $\mathbf{f}_{\underline{\rho}}$:

$$\mathbf{f}_{\underline{\rho}} = \left[f_{\underline{\rho}1} \; f_{\underline{\rho}2} \; f_{\underline{\rho}3} \; f_{\underline{\rho}4} \; f_{\underline{\rho}5} \; f_{\underline{\rho}6} \right]^T,$$

$$\mathbf{f}_{\overline{\rho}} = \left[f_{\overline{\rho}1} \; f_{\overline{\rho}2} \; f_{\overline{\rho}3} \; f_{\overline{\rho}4} \; f_{\overline{\rho}5} \; f_{\overline{\rho}6} \right]^T,$$

$$\mathbf{f} = \mathbf{f}_{\underline{\rho}} + \mathbf{f}_{\overline{\rho}}. \tag{4.17}$$

The general forces $\mathbf{f}$ need to be in operational space so that the pseudo mass matrix Λ, the Coriolis force μ, and gravity ρ must be in the operational space form as well. The Jacobian of joint limit transforms the general force to joint torques $\boldsymbol{\gamma}_{lim}$ as

$$\boldsymbol{\gamma}_{lim} = J_{lim}^T \left(\Lambda_{lim} \mathbf{f} + \rho_{lim} + \mu_{lim} \right), \tag{4.18}$$

$$\Lambda = \left(J A^{-1} J^T \right)^{-1},$$

$$\mu = J^T \mathbf{b} - \Lambda \dot{J} \dot{\mathbf{q}},$$

$$\rho = J^T \mathbf{g}. \tag{4.19}$$

The columns of the Jacobian represent the joints of the robot and the row represents the number of joints hitting the joint limit. For example,

$$J_{lim} = \left[0 \; 1 \; 0 \; 0 \; 0 \; 0 \right], \tag{4.20}$$

shows the Jacobian of the second joint hitting to its limit. By Equation (4.2), the computation of the null space matrix can be done as

$$\overline{J}_{lim} = A^{-1} J_{lim}^T \Lambda,$$

$$N_{lim} = I_{6\times 6} - J_{lim}^T \overline{J}_{lim}^T. \tag{4.21}$$

Once the repulsive torques are applied to each joint, the link will be pushed away from the critical zone. The control system will then switch back to the normal operational space control. The operational space control then computes a new trajectory based on the current position of the end-effector and the desire position.

CHAPTER 5

Result and Discussion

The optimization and simulation were coded in MATLAB. The optimization process uses the built-in function "fmincon" to find the minimum of the constrained nonlinear multivariable function. The integration is performed by a variable time step algorithm ode45 in MATLAB in order to find out the angle and velocity for each joint. The animation can be produced based on the angle of each joint to check for collisions using the Gilbert-Johnson-Keerthi (GJK) distance algorithm [2].

5.1 Optimization Result

Figure 5.1 shows the top view of the surgery workspace with the haptic device workspace after optimization. The specific values of the optimal location are given in Table 5.1.

Variables	Left-Hand Device	Right-Hand Device
X	$0.586m$	$0.554m$
Y	$0.291m$	$-0.297m$
Z	$0.059m$	$0.047m$
γ	$198.52°$	$0.02°$

Table 5.1: Optimization Result

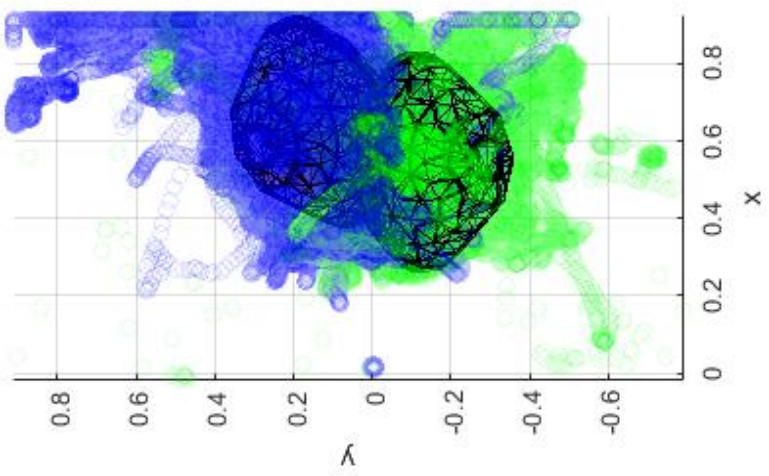

Figure 5.1: Optimization Result

By inspection, the workspace of haptic device from the optimal position can overlap with the main surgery workspace. The coverage rate is the ratio of the total amount of the position records measured from the surgeons over the number of the position records covered by the haptic device workspace from its optimal location. There are 16 subjects used for this analysis. Table 5.2 shows the coverage rates for all 16 subjects.

The average coverage rate is about 88.24 % and there are only three subjects below the average. Therefore, the placement optimization is valid to maximize the coverage and determine the optimal location.

5.2 Simulation Result

The dynamic model used operational space control to simulate the motion of haptic devices. The end-effector of the haptic device moved through the trajectories measured from surgeons. The joint limit constraint was activated properly to push

Subject	Coverage Rate (%)
2	89.86
4	93.87
5	65.45
10	59.26
11	96.86
15	91.95
18	88.81
20	90.56
22	97.59
23	91.75
24	91.45
25	96.92
27	93.41
28	92.00
29	75.23
30	96.90

Table 5.2: Coverage Rate for Each Subject

back the link when it approached to its bound. Therefore, the simulation provides a continuous motion trajectory which can be used to check the collision between two devices. In MATLAB, each link of haptic device has its own collision box. The GJK Algorithm is the method of determining the minimum distance between two convex sets, which can be used to check the collision between two collision boxes [2]. Table 5.3 shows the collision check result.

The collision check result shows that there was 1 collision detected in Subject 5 based on the trajectory by the simulation. For the left subjects, there were no collision

Subject	Times
2	0
4	0
5	1
10	0
11	0
15	0
18	0
20	0
22	0
23	0
24	0
25	0
27	0
28	0
29	0
30	0

Table 5.3: Collision Check Result

detected. Therefore, the simulation is valid to determine the possible motions of the haptic device and check the collision between the left-hand and the right-hand devices.

5.3 Preliminary Testing

After finishing optimization and simulation, it is important to test the result under the optimized interface to validate whether the method is useful or not. The preliminary testing was done with a surgeon who never participated in this study before. The surgeon successfully performed the suturing using the tools which were

connected with the haptic device. The haptic device had some limitations, which restricted the motion of the hands. This issue is possible to be solved in future work.

CHAPTER 6

CONCLUSION AND FUTURE WORK

This work measured the surgery workspace and defined the haptic device workspace. The placement optimization aimed to find the position and orientation of the haptic devices that would allow the greatest coverage of workspace measured form the surgeons. The cost function was the sum of distance between the position records outside the haptic device workspace and the end effector. As the sum of distance decreased, the haptic device workspace covered more position records, which meant the coverage of the surgery workspace increased. The dynamic model of the haptic device was created and used operational space control to follow the trajectory measured from the surgeons. The joint limit constraint played an important role to correct the trajectory when the links approached to their own bounds. The simulation results were used for the collision check. There was only 1 collision detected. Some preliminary testing was done with actual surgeons, which demonstrated that the optimization result was valid and useful for the haptic interface design.

The question remains related to the fact that the operational space control only controls the translational position of the end-effector. The haptic device has 6 DOFs and the operational space control only controls 3 DOFs translation, which means the motion path planned was not the unique solution. The simulation result just provides one possible motion. It is not guaranteed that the surgeon would follow the same path. Future work in simulation is to use operational space control to control not only the translation but also the orientation of the end-effector in order to find the

unique configuration such that the simulation can perfectly mimic the real surgery motion.

Finally, it is desirable to invite more surgeons to do the preliminary testing under the optimized haptic interface. The users' feedback will be very helpful to improve the optimization. These improvements will be pursued in our future work.

REFERENCES

[1] A. Bowling. *Vector Mechanics: A Systematic Approach*. Aqualan Press, LLC, 2018.

[2] S. Cameron. Enhancing gjk: computing minimum and penetration distances between convex polyhedra. 4:3112–3117 vol.4, 1997.

[3] Kyong-Sok Chang and O. Khatib. Operational space dynamics: efficient algorithms for modeling and control of branching mechanisms. 1:850–856 vol.1, 2000.

[4] M. Dinsmore, N. Langrana, G. Burdea, and J. Ladeji. Virtual reality training simulation for palpation of subsurface tumors. pages 54–60, 1997.

[5] Randy S. Haluck and Thomas M. Krummel. Computers and Virtual Reality for Surgical Education in the 21st Century. *Archives of Surgery*, 135(7):786–792, 07 2000.

[6] Northern Digital Inc. *3D Guidance API Guide*. 3 edition, 2017.

[7] Alireza Khatamian. Solving kinematics problems of a 6-dof robot manipulator. 2015.

[8] O. Khatib. A unified approach for motion and force control of robot manipulators: The operational space formulation. *IEEE Journal on Robotics and Automation*, 3(1):43–53, 1987.

[9] Wee Khor, Benjamin Baker, Kavit Amin, Adrian Chan, Ketan Patel, and Jason Wong. Augmented and virtual reality in surgery-the digital surgical environment: Applications, limitations and legal pitfalls. *Annals of Translational Medicine*, 4:454–454, 12 2016.

[10] Hyunyoung Lee, Byungsik Cheon, Minho Hwang, Donghoon Kang, and Dong-Soo Kwon. A master manipulator with a remote-center-of-motion kinematic structure for a minimally invasive robotic surgical system. *The International Journal of Medical Robotics and Computer Assisted Surgery*, 14:e1865, 10 2017.

[11] Chaobin Li, Dangxiao Wang, and Yuru Zhang. ifeel3: A haptic device for virtual reality dental surgery simulation. pages 179–184, 2011.

[12] Jose San Martin and G. Triviño. A study of the manipulability of the phantom omni haptic interface. 2006.

[13] Juan D. Muñoz Osorio, Mario D. Fiore, and Felix Allmendinger. Operational Space Formulation Under Joint Constraints. Volume 5B: 42nd Mechanisms and Robotics Conference, 08 2018. V05BT07A022.

[14] Jun Nakanishi, Rick Cory, Michael Mistry, Jan Peters, and Stefan Schaal. Operational space control: A theoretical and empirical comparison. *The International Journal of Robotics Research*, 27(6):737–757, 2008.

[15] Dario Panariello, Teodorico Caporaso, Stanislao Grazioso, Giuseppe Di Gironimo, Antonio Lanzotti, Sebastian Knopp, Luigi Pelliccia, Mario Lorenz, and Philipp Klimant. Using the kuka lbr iiwa robot as haptic device for virtual reality training of hip replacement surgery. pages 449–450, 2019.

[16] Jan Peters and Stefan Schaal. Reinforcement learning by reward-weighted regression for operational space control. page 745–750, 2007.

[17] Thitipong Sansanayuth, Itthisek Nilkhamhang, and Kanokvate Tungpimolrat. Teleoperation with inverse dynamics control for phantom omni haptic device. pages 2121–2126, 2012.

[18] Richard M. Satava. Virtual reality, telesurgery, and the new world order of medicine. *Journal of image guided surgery*, Jan 1995.

[19] Alejandro Jarillo Silva, Omar A. Domínguez Ramirez, Vicente Parra Vega, and Jesus P. Ordaz Oliver. Phantom omni haptic device: Kinematic and manipulability. pages 193–198, 2009.

[20] Domenico Spensieri, Johan S. Carlson, Robert Bohlin, Jonas Kressin, and Jane Shi. Optimal robot placement for tasks execution. *Procedia CIRP*, 44:395–400, 2016. 6th CIRP Conference on Assembly Technologies and Systems (CATS).

[21] Ziv Yaniv, Emmanuel Wilson, David Lindisch, and Kevin Cleary. Electromagnetic tracking in the clinical environment. *Medical physics*, 36:876–92, 04 2009.

[22] Peng Yu, Junjun Pan, Hong Qin, Aimin Hao, and Haipeng Wang. Real-time suturing simulation for virtual reality medical training. *Computer Animation and Virtual Worlds*, 31, 09 2020.